UC Berkeley

UC Berkeley Previously Published Works

Title

A multi-scale comparison of modeled and observed seasonal methane emissions in northern wetlands

Permalink

https://escholarship.org/uc/item/7bw6g6wg

Journal

Biogeosciences, 13(17)

ISSN

1726-4170

Authors

Xu, Xiyan

Riley, William J

Koven, Charles D

et al.

Publication Date

2016

DOI

10.5194/bg-13-5043-2016

Peer reviewed

eScholarship.org Powered by the California Digital Library
University of California

Biogeosciences, 13, 5043–5056, 2016
www.biogeosciences.net/13/5043/2016/
doi:10.5194/bg-13-5043-2016
© Author(s) 2016. CC Attribution 3.0 License.

Biogeosciences Open Access EGU

A multi-scale comparison of modeled and observed seasonal methane emissions in northern wetlands

Xiyan Xu[1], William J. Riley[1], Charles D. Koven[1], Dave P. Billesbach[2], Rachel Y.-W. Chang[3,4], Róisín Commane[3], Eugénie S. Euskirchen[5], Sean Hartery[4], Yoshinobu Harazono[6,7], Hiroki Iwata[6,8], Kyle C. McDonald[9,10], Charles E. Miller[10], Walter C. Oechel[11,12], Benjamin Poulter[13], Naama Raz-Yaseef[1], Colm Sweeney[14,15], Margaret Torn[1,16], Steven C. Wofsy[3], Zhen Zhang[13,17], and Donatella Zona[11,18]

[1]Earth Sciences Division, Lawrence Berkeley National Laboratory, Berkeley, California, USA
[2]Biological System Engineering Department, University of Nebraska, Lincoln, Nebraska, USA
[3]School of Engineering and Applied Sciences, Harvard University, Cambridge, Massachusetts, USA
[4]Department of Physics and Atmospheric Science, Dalhousie University, Halifax, Nova Scotia, Canada
[5]Institute of Arctic Biology, University of Alaska Fairbanks, Fairbanks, Alaska, USA
[6]International Arctic Research Center, University of Alaska Fairbanks, Fairbanks, Alaska, USA
[7]Graduate School of Life and Environmental Sciences, Osaka Prefecture University, Sakai, Osaka, Japan
[8]Department of Environmental Sciences, Faculty of Science, Shinshu University, Matsumoto, Nagano, Japan
[9]Department of Earth and Atmospheric Sciences, CUNY Environmental Crossroads Initiative and NOAA-CREST Institute, The City College of New York, City University of New York, New York, USA
[10]Jet Propulsion Laboratory, California Institute of Technology, Pasadena, California, USA
[11]Global Change Research Group, Department of Biology, San Diego State University, San Diego, California, USA
[12]Department of Environment, Earth and Ecosystems, The Open University, Milton Keynes, MK7 6AA, UK
[13]Department of Ecology, Montana State University, Bozeman, MT 59717, USA
[14]Cooperative Institute for Research in Environmental Sciences, University of Colorado, Boulder, Colorado 80304, USA
[15]NOAA Earth System Research Laboratory, Global Monitoring Division, Boulder, Colorado, USA
[16]Energy and Resources Group, University of California-Berkeley, Berkeley, California, USA
[17]Swiss Federal Research Institute WSL, Birmensdorf 8059, Switzerland
[18]Department of Animal and Plant Sciences, University of Sheffield, Sheffield, S102TN, UK

Correspondence to: Xiyan Xu (xxu@lbl.gov)

Received: 29 April 2016 – Published in Biogeosciences Discuss.: 9 May 2016
Revised: 5 August 2016 – Accepted: 24 August 2016 – Published: 13 September 2016

Abstract. Wetlands are the largest global natural methane (CH_4) source, and emissions between 50 and 70° N latitude contribute 10–30 % to this source. Predictive capability of land models for northern wetland CH_4 emissions is still low due to limited site measurements, strong spatial and temporal variability in emissions, and complex hydrological and biogeochemical dynamics. To explore this issue, we compare wetland CH_4 emission predictions from the Community Land Model 4.5 (CLM4.5-BGC) with site- to regional-scale observations. A comparison of the CH_4 fluxes with eddy flux data highlighted needed changes to the model's estimate of aerenchyma area, which we implemented and tested. The model modification substantially reduced biases in CH_4 emissions when compared with CarbonTracker CH_4 predictions. CLM4.5 CH_4 emission predictions agree well with growing season (May–September) CarbonTracker Alaskan regional-level CH_4 predictions and site-level observations. However, CLM4.5 underestimated CH_4 emissions in the cold season (October–April). The monthly atmospheric CH_4 mole fraction enhancements due to wetland emissions are also assessed using the Weather Research and Forecasting-Stochastic Time-Inverted Lagrangian Transport (WRF-STILT) model coupled with daily emissions from CLM4.5 and compared with aircraft CH_4 mole fraction mea-

surements from the Carbon in Arctic Reservoirs Vulnerability Experiment (CARVE) campaign. Both the tower and aircraft analyses confirm the underestimate of cold-season CH_4 emissions by CLM4.5. The greatest uncertainties in predicting the seasonal CH_4 cycle are from the wetland extent, cold-season CH_4 production and CH_4 transport processes. We recommend more cold-season experimental studies in high-latitude systems, which could improve the understanding and parameterization of ecosystem structure and function during this period. Predicted CH_4 emissions remain uncertain, but we show here that benchmarking against observations across spatial scales can inform model structural and parameter improvements.

1 Introduction

Natural wetlands are the largest natural methane (CH_4) source, contributing up to 34 % of global CH_4 emissions (Kirschke et al., 2013). Between 1980 and 2009, estimated global annual CH_4 emissions from wetlands varied from 115 to 231 Tg CH_4 in top–down atmospheric inversion models and 169 to 284 Tg CH_4 in bottom–up process-based land models (Kirschke et al., 2013). Peat-rich bogs and fens lying between 50 and 70° N constitute about half of the global wetland area and release 10–30 % of the total wetland CH_4 (Wania et al., 2010; Zhuang et al., 2004; Bergamaschi et al., 2009; Riley et al., 2011). Much of the northern wetland area is in the permafrost zone, which stores 1035 ± 150 Pg soil organic carbon for the 0–3 m soil depth (Hugelius et al., 2014). When permafrost soils thaw, CH_4 is produced under anaerobic conditions by methanogenic archaea. Once CH_4 is produced, it can be oxidized by methanotrophic archaea. CH_4 surface emissions occur through several transport pathways: aqueous and gaseous diffusion, ebullition, and aerenchyma diffusion and advection. At any point in the soil, the CH_4 concentration is governed by the balance between CH_4 production in anoxic zones, CH_4 consumption in oxic zones, transport, and atmospheric CH_4 diffusion at the soil–atmosphere interface.

Many interacting factors (e.g., temperature, thaw depth, soil moisture, depth of the water table, vegetation type) affect CH_4 production and emission. CH_4 production has a positive response to temperature increase (Van Hulzen et al., 1999; van Winden et al., 2012; Hommeltenberg et al., 2014), and laboratory incubations of soil samples from the active layer show that large variability of Q_{10} values for CH_4 production (1.5 to 28, Segers, 1998) is related to site-specific peatland type and organic matter quality (Lupascu et al., 2012). CH_4 emissions also show positive temperature dependence above freezing. The temperature dependence of surface CH_4 emission is much stronger than that of respiration and photosynthesis, which indicates increases in both CH_4 emissions and the ratio of CH_4 to CO_2 emissions with seasonal increases in temperature (Yvon-Durocher et al., 2014). The positive temperature dependence of CH_4 emissions may only be valid when CH_4 oxidation is less sensitive to temperature (van Winden et al., 2012). The Q_{10} value for CH_4 oxidation was reported to be 1.4 to 2.1 in northern peat soils (Dunfield et al., 1993). Strong oxidation temperature sensitivity can lead to decreased CH_4 surface emissions with rising temperature (Wang et al., 2014). The positive dependence of CH_4 emissions on soil temperature can be most significant in areas with sufficient soil moisture or a shallow water table (Roulet et al., 1992; Moosavi et al., 1996; Wickland et al., 1999). The dependency of CH_4 emissions on temperature can vanish at a high temperature and low water table (Hommeltenberg et al., 2014). At low water table levels, large CH_4 oxidation can mask the CH_4 production temperature sensitivity in the net emissions. CH_4 production under sub-zero temperatures was reported in incubation experiments (Clein and Schimel, 1995; Brouchkov et al., 2003); however, the mechanisms that regulate CH_4 production under cold temperatures have not been clarified.

Soil water content exerts a strong control on CH_4 emissions by affecting belowground carbon decomposition and root growth (Iversen et al., 2015). A lowered water table typically reduces CH_4 production and emission because of a higher aerobic-to-anaerobic respiration ratio in the soil column and CH_4 oxidation during diffusive transport through the oxygen-rich surface layer (Whalen and Reeburgh, 1990). If CH_4 produced in anoxic zones (e.g., below the water table) is transported to the atmosphere through aerenchyma, the impact of methanotrophy on net CH_4 emissions is diminished (Bartlett et al., 1992; Torn and Chapin, 1993; King et al., 1998; Juutinen et al., 2003; McEwing et al., 2015). The reduced methanotrophic impacts vary with vascular species cover and root density and are more common in tall vegetation because taller plants have more extensive root systems that enable more methanogenesis and pore water CH_4 to escape to the atmosphere (van Fischer et al., 2010). The correlation between water table depth and CH_4 emission can be very weak if the water table drops in an already oxic surface layer (Sturtevant et al., 2012).

The seasonal cycle of CH_4 emissions and their physical controls are strongly controlled by the freeze–thaw cycle in northern wetlands and regulation of wetland extent. The northern wetland area retrieved from the 19 and 37 GHz passive microwave Special Sensor Microwave/Image (SSM/I) brightness temperature database shows that maximum inundation is usually observed during July, August and September in North America (48–68° N) and between June and September in northern Eurasia (Mialon et al., 2005). The inundation dynamics retrieved from the Special Sensor Microwave Imager (SSM/I) and the International Satellite Cloud Climatology Project (ISCCP) observations, European Remote Sensing (ERS) scatterometer responses, and Advanced Very High Resolution Radiometer (AVHRR) visible and near-infrared reflectance also show that maximum in-

undation occurs in July and August in northern boreal regions (55–70° N; Prigent et al., 2007). The inferred wetland extent increases rapidly during the spring thaw period and shrinks again during the fall freeze period, though it is unclear on large scales how much of this seasonal cycle is due to changes in the areal fraction of land in which water ponds at the surface versus changes in the phase of that water. The interannual variability of high-latitude summer wetland extent is very small. Larger interannual variability during the intermediate seasons arises from the large variability of the timing and extent of snowmelt and accumulation (Mialon et al., 2005). For boreal bogs north of 50° N, the variation in wetland area contributed about 30 % to the annual emissions and can explain the interannual variation in regional CH_4 emissions (Ringeval et al., 2010).

Site measurements have shown great variability in seasonal CH_4 emissions (Wilson et al., 1989; Mastepanov et al., 2008; 2013; Zona et al., 2016). In the late fall to winter, the surface water or shallow peat zone are frozen, and CH_4 produced below the frozen layer can be trapped. Only a small portion of the trapped CH_4 is oxidized because of low oxygen concentrations below the frozen layer (Mastepanov et al., 2008). Observed CH_4 emissions during spring thaw are highly variable and contribute substantially to total annual emissions. CH_4 fluxes during the spring thaw period contributed 11 % to the annual budget over an aapa mire in Finnish Lapland (Hargreaves et al., 2001). The emission amounts can be 24 % of the total annual emissions during the spring period after snowmelt next to an open pool in Caribou Bog, Maine, while the proportion can be as high as 77 % in the adjacent upland area (Comas et al., 2008). In the non-inundated upland tundra, the cold-season (September to May) emissions account for more than 50 % of the annual CH_4 emissions (Zona et al., 2016). Although wetlands can contribute a large proportion of annual CH_4 emissions during the cold season, the seasonal peak of CH_4 emissions is usually observed in the summer (Pickett-Heaps et al., 2011; Zona et al., 2016). A transport model combined with flight measurements showed the peak CH_4 emission to be in July–August in the Hudson Bay Lowlands (Pickett-Heaps et al., 2011). Although the recorded emission pulses during spring thaw and late fall (Song et al., 2012; Tokida et al., 2007; Rinne et al., 2007; Mastepanov et al., 2008, 2013) may be more localized and of minor importance to annual emissions (Chang et al., 2014; Rinne et al., 2007), the pulses indicates the complexity and heterogeneity in the seasonal CH_4 cycle.

Many modeling studies have shown that there is large uncertainty in predictions of spatial patterns of CH_4 emissions from natural wetlands on the regional and global scales (Melton et al., 2013; Bohn et al., 2015). This uncertainty can be roughly split into poor knowledge of water table and soil moisture dynamics versus poor knowledge of CH_4 fluxes per unit area of land with a given water table depth or soil moisture state; both contribute substantially to the overall uncertainty. One approach to reducing this overall uncertainty is to focus on the seasonal cycles of CH_4 emissions on the site scale (where inundation dynamics can be more easily constrained) versus on larger scales to ask whether model predictions and errors are consistent across these scales. The temporal dynamics of CH_4 emissions over the season cannot be ignored when calculating long-term CH_4 budgets (Morin et al., 2014). To investigate the seasonal cycle of CH_4 emissions in northern wetlands and the underlying processes in a climate model context, we evaluated and modified the CH_4 biogeochemistry module in the Community Land Model (CLM 4.5). Seasonal cycles of CH_4 emissions in Alaskan wetlands are analyzed based on the modified model predictions, CH_4 emission measurements at high-latitude sites, CarbonTracker CH_4 emission estimates and atmospheric inversion estimates of surface CH_4 emissions from data collected in the Carbon in Arctic Reservoirs Vulnerability Experiment (CARVE). The models and data are described in Sect. 2. Multi-scale comparison results and discussions are given in Sect. 3 and concluding remarks in Sect. 4.

2 Data and methods

2.1 Model descriptions

2.1.1 CH_4 model in CLM4.5-BGC

The CH_4 biogeochemistry model used here (CLM4Me; Riley et al., 2011) has been coupled to the revised land model CLM4.5, which includes numerous changes to vegetation, soil biogeochemistry and hydrology from the CLM4.0 in which CLM4Me was originally developed. CLM4Me includes the representation of CH_4 production, oxidation and transport through the soil column. Transport includes multiple pathways: aerenchyma transport, ebullition, and aqueous and gaseous diffusion. Aerenchyma is the most efficient pathway for gas exchange between the soil and atmosphere in wetlands or aquatic environments, through which atmosphere O_2 is supplied to roots and the rhizosphere while CH_4 is removed from the soil to shoots and the atmosphere. In CLM4Me, aerenchyma transport (A) is parameterized as gaseous diffusion in response to a concentration gradient between the soil layer (z) and the atmosphere (a) as

$$A = \frac{C(z) - C_a}{\frac{r_L z}{D p^T \rho_r} + r_a}, \quad (1)$$

where D ($m^2\ s^{-1}$) is the free-air gas diffusion coefficient, C (z; $mol\ m^{-3}$) is the gaseous concentration at depth z, dimensionless r_L is the ratio of total root length to root depth, p (−) is tiller porosity, T ($m^2\ m^{-2}$) is specific aerenchyma area, r_a ($s\ m^{-1}$) is the aerodynamic resistance between the surface and the atmospheric reference height and r_L (−) is the root mass fraction in the soil layer. The aerenchyma area T is sea-

sonally varying with phenology S (described below):

$$T = \frac{f_N N_a S}{0.22} \pi R^2, \quad (2)$$

where N_a (g C m^{-2}) is annual net primary production (NPP), R (2.9×10^{-3} m) is the aerenchyma radius, f_N is the belowground fraction of current NPP, and the factor 0.22 (g C) is the mass of C per tiller. The dimensionless term S is included in CLM4Me to capture seasonal cycles of aerenchymous tissues. In the absence of data on phenology of aerenchyma, S was originally taken as the leaf area index (LAI).

The default method for calculating inundation fraction (F_{def}) remains the same as described in Riley et al. (2011), which applied a simple inversion model to represent the spatial inundation:

$$F_{def} = p_1 e^{-z_w/p_2} + p_3 Q_r. \quad (3)$$

The three parameters (p_1, p_2, p_3) are optimized with the inundation map by Prigent et al. (2007). z_w is simulated water table depth (m) and Q_r is surface runoff (mm s^{-1}). We also applied an estimate of inundation fraction F_{S+G} derived from seasonal cycle of inundation fraction from the Surface WAter Microwave Product Series Version 2.0 (SWAMPS; Schroeder et al., 2015) developed at the NASA Jet Propulsion Laboratory with the Global Lakes and Wetlands Dataset (GLWD; Lehner and Doll, 2004) to discuss the potential uncertainties in CH_4 emissions caused by wetland area.

Our model is driven by half-degree CRUNCEP V5 6-Hourly Atmospheric Forcing dataset (1901–2013; http://esgf.extra.cea.fr/thredds/fileServer/store/p529viov/cruncep/readme.htm). Monthly wetland CH_4 emissions are simulated between the year 2000 and 2012 during which F_{S+G} is available. The monthly CH_4 emissions in half-degree resolution are regridded to $1^\circ \times 1^\circ$ and averaged longitudinally to compare with CarbonTracker-predicted CH_4 fluxes. Daily wetland CH_4 emissions are simulated for the years 2012 and 2013 to calculate the atmospheric enhancements of CH_4 due to modeled surface emissions.

2.1.2 WRF-STILT modeling of CH_4 transport

We simulate the atmospheric CH_4 mole fraction enhancements due to wetland emissions by combining the CLM4.5-predicted daily surface emissions with the land surface influences ("footprint") calculated by the Weather Research and Forecasting-Stochastic Time-Inverted Lagrangian Transport (WRF-STILT) model (Henderson et al., 2015). WRF-STILT estimates the upwind surface influence along the flight track of the CARVE aircraft by releasing 500 particles at the point of flight measurement and allowing them to stochastically disperse in reverse time over 10 days (Henderson et al., 2015). The resolution of the resulting footprint sensitivity used in this study is $0.5^\circ \times 0.5^\circ$, covering 30–90° N, circumpolar. However, we assume that CH_4 transported from areas outside of Alaska are most likely mixed thoroughly in the atmosphere before they reach Alaska and therefore only contribute to the background abundance of CH_4.

2.2 Measurements of CH_4

2.2.1 Site-scale observations

We compare CLM4.5 CH_4 emission predictions with data obtained from published studies and recent measurements of Northern Hemisphere static-chamber (SC) measurements at 10 sites and eddy covariance (EC) measurements at 10 sites, of which 8 are in Alaska (Supplement Table S1). The eddy covariance measurements in Alaska (Fig. S2) are obtained at the Barrow Environmental Observatory (BEO1) tower operated by the Next Generation Ecosystem Experiment (NGEE)-Arctic group; the Barrow Environmental Observatory tower (BEO2), the Biocomplexity Experiment South (BES) tower, the Climate Monitoring and Diagnostics Laboratory (CMDL) tower, the Atqasuk (ATQ) tower and the Ivotuk (IVO) tower operated by Global Change Research Group at San Diego State University (Zona et al., 2016); the tower in Fairbanks (FAI; Iwata et al., 2015) operated by the International Arctic Research Center, the University of Alaska Fairbanks; and the tower at the Imnavait Creek watershed (IMN; Euskirchen et al., 2012). Monthly means are calculated across each observational record to compare to the predicted mean seasonal CH_4 cycle. We discarded the monthly mean if the number of valid measurement days is less than half a month.

2.2.2 Comparisons to airborne measurements

The regionally integrated CH_4 mole fraction enhancements over Alaska were calculated from the CH_4 mole fractions measured by NOAA and Harvard Picarro spectrometers aboard a NASA C-23B aircraft (N430NA) during CARVE aircraft flights (Chang et al., 2014). The Harvard CH_4 measurements were gap filled with the NOAA CH_4 measurements to create a continuous 5 s time series. The flight measurements were conducted on selected days from May to September in 2012 and April to October in 2013 during the Carbon in Arctic Reservoirs Vulnerability Experiment (CARVE) campaign for a total of 31 flight days in 2012 and 43 flight days in 2013 (Supplement Fig. S1 and Table S2). The measurements of CH_4 with concurrent CO mole fractions above 150 ppb are excluded to remove possible CH_4 production from biomass burning. In Alaska, atmospheric boundary layer depth is in the range of 1100–1600 m above ground level (a.g.l.) during April and October according to COSMIC satellite and Radiosonde data (Chan and Wood, 2013). We assume that the observed concentration fluctuations below 500 m a.g.l. can be used to infer the variation of surface CH_4 fluxes; the measurements above 1600 m a.g.l. are used to infer the background mole fraction of CH_4.

The monthly mean enhancements in observed atmospheric CH_4 mole fraction are compared to that estimated from the CLM4.5 CH_4 enhancements.

2.2.3 Comparisons to global-scale inversions

To compare our methane emissions with global- and regional-scale inversions, we use monthly regional CH_4 emissions predicted by CarbonTracker (Peters et al., 2007; Bruhwiler et al., 2014) at $1^\circ \times 1^\circ$ resolution. In CarbonTracker estimates, the natural CH_4 emissions correspond to wetlands, soils, oceans, insects and wild animals. To examine the land CH_4 emissions only, we apply the CLM land mask to exclude the inferred CarbonTracker CH_4 emission from the ocean surface. CarbonTracker CH_4 estimates are available from January 2000 through December 2010; we therefore limit comparisons against the CLM4.5 predictions to this period.

3 Results and discussion

3.1 Model constraints and comparison with observations

We performed sensitivity analyses of all the parameters affecting seasonal CH_4 production, oxidation and emission pathways and found that the parameterization of aerenchyma transport has the greatest impact on the seasonal CH_4 emissions in saturated areas. The CH_4 surface flux sensitivity to aerenchyma is most sensitive to aerenchyma area in saturated conditions and decreases with increasing aerenchyma area because increased O_2 fluxes through aerenchyma cause more CH_4 oxidation in the rhizosphere (Riley et al., 2011). Meng et al. (2012) tested plant-functional-type (pft)-specific fine-root carbon (C_{FR}) as a proxy of aerenchyma area and found that aerenchyma area dependence on C_{FR} leads to about 39 % increases in global annual CH_4 emissions. In that study, an early spring spike in CH_4 emission through aerenchyma transport was shown at a Michigan site in both LAI and C_{FR}-based aerenchyma area. Our analysis shows that the simulated CH_4 burst through aerenchyma transport during spring thaw is very common in areas experiencing winter dormancy. In CLM4.5, CH_4 production in a given volume of soil is proportional to heterotrophic respiration (HR) in that soil volume, adjusted by soil temperature, pH, redox potential and variation of seasonal inundation fraction. In the model, CH_4 production starts when the soil temperature is above the freezing point. However, CLM4.5 LAI lags behind the primary thaw day, which, because the original representation of aerenchyma in CLM4.5 is tied directly to LAI, results in a very low aerenchyma area and thus low aerenchyma transport of O_2 into the soil during the spring thaw period. Only a very small portion of the CH_4 produced in the soil column is oxidized, allowing a large fraction of CH_4 to be transported to the surface by aerenchyma. The low oxidation rate also occurs when aerenchyma area is calculated with C_{FR}.

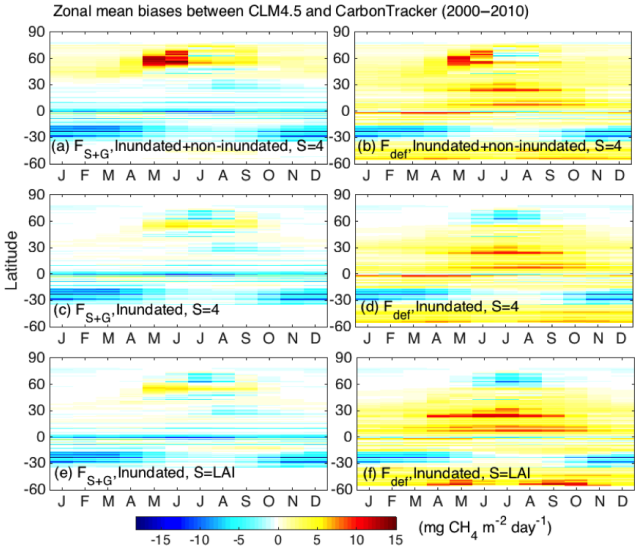

Figure 1. Zonal mean biases of CH_4 emissions between CLM4.5 predictions and CarbonTracker (CH_4_CLM4.5-CH_4_CarbonTracker) with SWAMPS-GLWD (F_{S+G}) and CLM4.5 predicted (F_{def}) inundation fraction: CLM4.5 predictions of both inundated and non-inundated emissions with F_{S+G} **(a)** and F_{def} **(b)**, while aerenchyma area is corrected with $S = 4$; CLM4.5 predictions of inundated emissions only with F_{S+G} **(c)** and F_{def} **(d)**, while aerenchyma area is corrected with $S = 4$; CLM4.5 predictions of inundated emissions only with F_{S+G} **(e)** and F_{def} **(f)**, while aerenchyma area is parameterized by default $S = \mathrm{LAI}$.

The uncertainty in representing the seasonality of aerenchyma area is due to (1) a poor current understanding of root dynamics and their control on aerenchyma area and (2) scant relevant observations. In tundra, the aboveground production is often not a good proxy for belowground production because the soil temperature peaks later in the growing season than solar irradiance (Sullivan and Welker, 2005; Sloan, 2011). Further, root dynamics are strongly species dependent. Root growth of *Eriophorum angustifolium* may not be delayed when soil temperature is near 0 °C (Chapin, 1974; Billing et al., 1977), while *Dupontia fischeri* produces many fewer root tips at these low temperatures. In *Eriophorum vaginatum*, fine-root growth lags significantly behind the aboveground spring growth flush (Kummerow and Russell, 1980).

To eliminate the possible bias in the seasonal variation of roots and the extremely low oxidation rate which caused CLM4.5 to predict a large CH_4 burst from inundated areas during the spring thaw, we modified the model parameter S to be constant, which is used in the aerenchyma area estimation. We constrained S using global total CH_4 emissions estimated by top–down and bottom–up simulations during

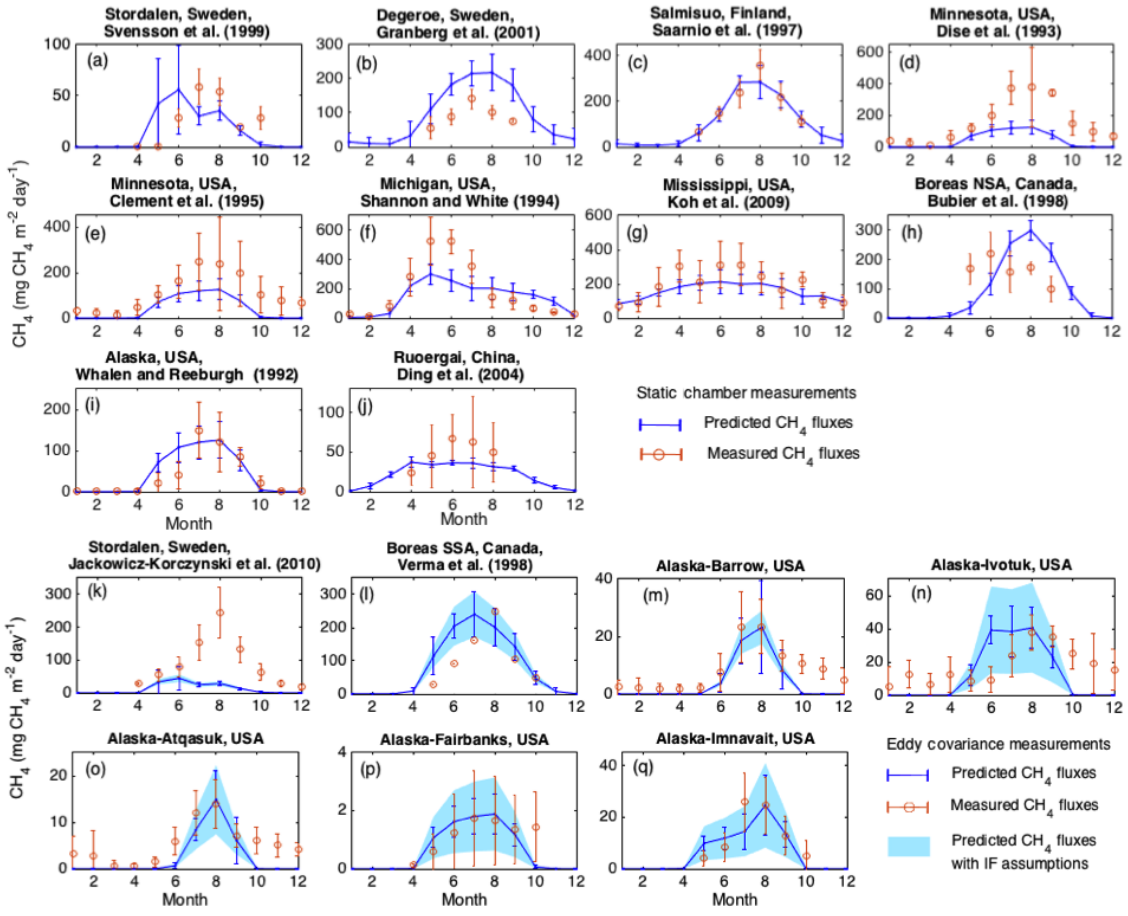

Figure 2. Comparison of monthly mean simulated net CH_4 flux between 2000 and 2012 and observed monthly mean net CH_4 emissions in measurement year(s). The site measurements with static chamber are shown in **(a)**–**(j)**, and measurements with eddy covariance (EC) towers are shown in **(k)**–**(q)**. The error bars are standard deviation of monthly mean. The measurements with EC tower are weighted with a range of inundation fraction (IF) based on best estimates available: Stordalen – 80–100 %; Boreas SSA – 50–90 %; Alaska-Barrow – 60–100 %; Alaska-Atqasuk – 10–30 %; Alaska-Ivotuk – 5–25 %; Alaska-Fairbanks – 0.5–2.5 %; Alaska-IMN – 5–25 %. Detailed description of the sites and measurements are shown in Table S1.

2000–2009 (Kirschke et al., 2013) and site-level measurements. We exclude the CH_4 emission from non-inundated areas for the analysis of seasonal dynamics because the model shows a very small seasonal contribution of CH_4 emissions from non-inundated areas globally (Fig. 1). This CH_4 emission pulse from non-inundated areas, which may be related to soil moisture anomalies during spring thaw, has not been experimentally validated but can lead to large biases in simulated CH_4 emissions from northern high latitudes ($>50^\circ$ N) in May and June (Fig. 1a and b). This simplification of the model-produced seasonal cycles that did not contain the large springtime CH_4 emission bursts, and we therefore used this modified version for all experiments here.

We assessed the sensitivity of the modeled CH_4 fluxes to parametric uncertainty in the constant dimensionless factor S, as described above. S has a direct effect on the magnitude of modeled CH_4 emissions via its control of oxygen diffusion through the soil column and thus CH_4 oxidation. When $S = \mathrm{LAI}$, the very low LAI in the spring thaw period leads to low oxidation and consequently overestimated CH_4 net emissions compared to CarbonTracker predictions. During the growing season, the model overestimates LAI at high latitude (Tian et al., 2004) leading to high oxidation and consequently underestimated net CH_4 emissions (Fig. 1e and f). However, few observations of aerenchymous tissue biomass are available to provide an a priori constraint to this value. Our goal here is to use a reasonable value of this parameter, not to fully characterize the uncertainty of the parameter choice on CH_4 emissions.

Based on a comparison of the globally integrated CH_4 flux with other global estimates, we choose $S = 4$, which resulted in an estimated annual total CH_4 emission of 228 (interannual variability (IAV): 221–239) Tg CH_4 yr^{-1} with F_{def} and 206 (IAV: 200–217) Tg CH_4 yr^{-1} with F_{S+G} dur-

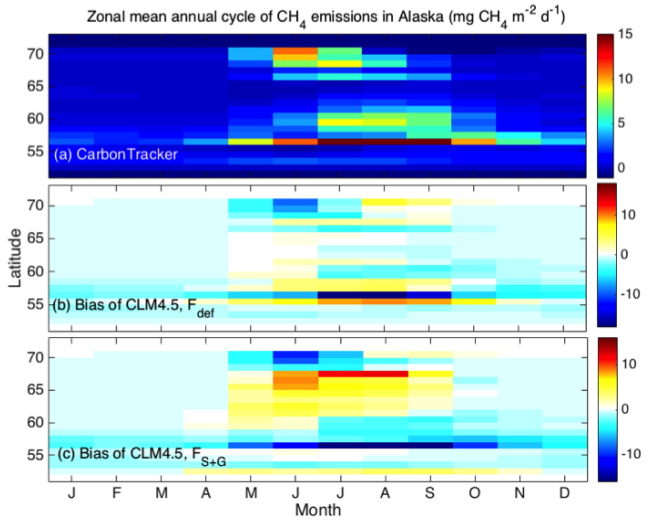

Figure 3. The 2000–2010 zonal mean annual cycle of CH_4 emission ($mg\,CH_4\,m^{-2}\,day^{-1}$) across Alaska predicted by CarbonTracker **(a)** and biases of CLM4.5 with CLM4.5-predicted inundation fraction (F_{def}) **(b)** and SWAMPS-GLWD inundation fraction (F_{S+G}; **c**). The $0.5^\circ \times 0.5^\circ$ CLM4.5 is regridded to $1^\circ \times 1^\circ$ to be consistent with CarbonTracker.

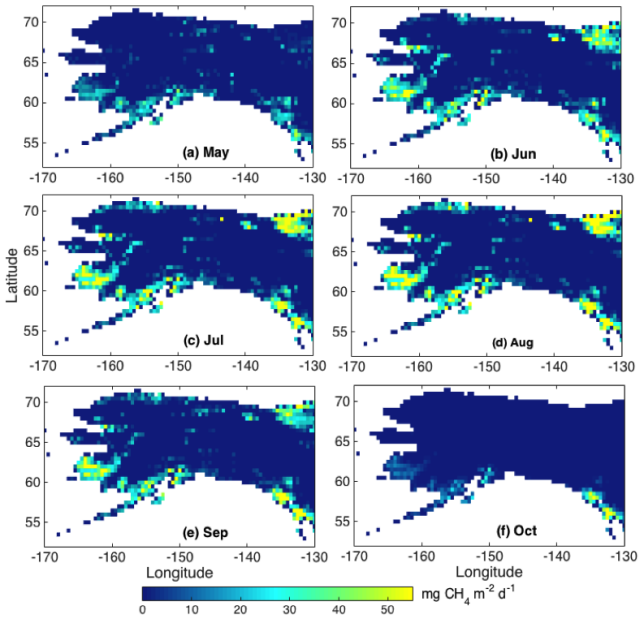

Figure 4. CLM4.5 simulated mean monthly CH_4 emissions with F_{def} across years 2000–2012.

ing the period 2000–2009. The top–down and bottom–up models provide estimates of CH_4 emissions from natural wetlands of 175 (IAV: 142–208) $Tg\,CH_4\,yr^{-1}$ and 217 (IAV: 177–284) $Tg\,CH_4\,yr^{-1}$, respectively, during the same period (Kirschke et al., 2013). The mean CH_4 emission predicted by CLM4.5 is about 42 $Tg\,CH_4\,yr^{-1}$ lower than the original CLM4Me prediction (annual mean of 270 $Tg\,CH_4\,yr^{-1}$ from 1948 to 1972) but slightly larger than the mean value from other bottom–up and top–down models. The disagreement between studies with different models is as large as 66 % (Kirschke et al., 2013); hence, our estimate is well within the range of values from top–down constraints and underscores the uncertainty involved in using such a constraint in inferring model parameters.

Compared with CarbonTracker predictions, CLM's biases of underestimated growing season CH_4 emissions north of 56° N and biases of overestimated CH_4 emissions in 2–53° N and 34–56° S are reduced when using $S = 4$ compared to the default parameterization (Fig. 1d and f). For the global zonal mean, the CLM CH_4 prediction biases are reduced with F_{S+G} (RMSE = 2.5 $mg\,CH_4\,m^{-2}\,day^{-1}$) compared with F_{def} (RMSE = 3.1 $mg\,CH_4\,m^{-2}\,day^{-1}$). With F_{S+G}, the biases are much reduced in 2–50° N and 30–58° S. However, negative CH_4 emission biases in the tropics remain (Fig. 1c and e). The differences in CH_4 emissions using SWAMPS-GLWD and CLM4.5-predicted inundation fraction implies that the prediction uncertainties are not only from the biogeochemical parameterization but also from the wetland extent, consistent with several recent model intercomparison analyses (Melton et al., 2013; Bohn et al., 2015). In Alaska, the predicted annual CH_4 emissions between 2000 and 2010 are 1.47 ± 0.20, 1.58 ± 0.07 and $1.12 \pm 0.05\,Tg\,CH_4\,yr^{-1}$ for CarbonTracker, CLM4.5 with F_{S+G} and CLM4.5 with F_{def}, respectively. Although our predicted annual emissions are reasonable compared with most land surface model predictions, the May to September predictions are about 50–70 % of the emissions estimated using an atmospheric inversion based on CARVE observations of $2.1 \pm 0.5\,Tg,CH_4\,yr^{-1}$ (Chang et al., 2014).

3.2 Seasonal CH_4 emissions

3.2.1 Site-level comparison

The mean seasonal cycle of predicted CH_4 emissions is calculated from the 2000–2012 monthly mean in a $0.5^\circ \times 0.5^\circ$ grid cell where site measurements exist, while the seasonal cycle of site measurements is calculated for the measurement years. If multiple measurement sites and multiple measurement years with the same measurement method (SC or EC) exist within a given grid cell, the observations are averaged to create a grid cell mean value that can be directly compared with the modeled value for that grid cell. In the 10 site-level static-chamber measurements at saturated sites (Fig. 2a–l), the seasonality is well predicted by the revised CLM4.5 CH_4 model at most sites. Measurements and predictions show the peak emission month to be July or August at most sites, except the site in Michigan, USA (Fig. 2f), where the model successfully predicted the peak emissions in May. However, the model misrepresents the seasonality at the Stordalen (Sweden; Fig. 2a and k) and the Boreas NSA

(northern study area) (Canada; Fig. 2i) site. At the Ruoergai site (China; Fig. 2j), the model does not show a strong seasonal variation from April to September and notably underestimates the growing season CH_4 emissions. The underestimation of growing season emissions is also found at the Minnesota (USA), Michigan (USA) and Boreas NSA (Canada) sites (Fig. 2d, e, f and h). The sites experiencing soil frost with valid measurements in the cold season demonstrate the CLM4.5 underestimation of CH_4 emissions during this period (Fig. 2a, d, e and i).

The eddy covariance measurements from four sites – the BEO1, BEO2, BES and CMDL sites – are in the same model grid cell; therefore, the measurements in these four sites are aggregated to the same grid cell as that of Alaska (Fig. 2m). As the footprints of the measurement towers were not estimated, all the modeled CH_4 emissions at eddy covariance sites are weighted with an observationally estimated seasonally invariant range of inundation faction: Stordalen – 80–100 %; Boreas SSA (southern study area) – 50–90 %; Barrow – 60–100 %; Atqasuk – 10–30 %; Ivotuk – 5–25 %; Fairbanks – 0.5–2.5 %; and IMN – 5–25 %. Measurements at the Stordalen site (Fig. 2a and k) show very different CH_4 emission patterns in seasonality and magnitude for different years and measurement methods. The model significantly underestimates CH_4 emissions even with the maximum fraction of inundation in Stordalen (Fig. 2k). In comparison with the static-chamber measurements at Alaska (Fig. 2h), the model predicts a much shorter CH_4 emission season at the non-inundated sites (Fig. 2m–q). The estimated CH_4 emissions begin in April at Ivotuk, Fairbanks and Imnavait. At the northern sites, Barrow and Atqasuk, the estimated CH_4 emissions begin in May. In the short emission season, the model underestimates CH_4 emissions in June and July at Barrow and Atqasuk and in July at Imnavait, even with the maximum inundation estimation. While the cold-season measurements at Barrow, Atqasuk and Ivotuk show large CH_4 emissions from October to April in agreement with the static-chamber measurements at the sites with cold-season soil frost, predicted CH_4 emissions end in October at all the Alaskan sites. The largest monthly mean emissions in Alaska cold season are $24.8 \pm 9.0\,\mathrm{mg\,CH_4\,m^{-2}\,day^{-1}}$ measured in October at Ivotuk.

A number of factors affect the correspondence between site-level CH_4 emission observations and CLM4.5 predictions (Fig. 2), including (1) that we used reanalysis climate forcing data which may lead to some of the differences with the site observations; (2) that we used the model's default surface characterization, which is unlikely to exactly match the actual vegetation and soil properties; (3) that the spatial and temporal coverage of the site data are sparse; (4) that the interannual variation of wetland CH_4 emission can be significant; (5) that the method of measuring CH_4 fluxes varied from site to site and (6) that the seasonal fraction of inundation in the eddy covariance tower footprint is unknown. We also expect differences between our CLM4.5 predictions

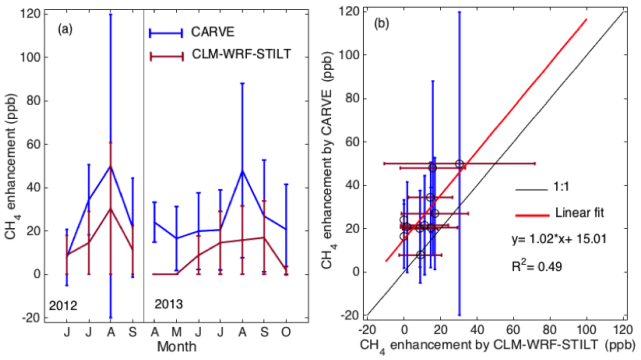

Figure 5. The monthly mean atmospheric mole fraction enhancements in CH_4 estimated by WRF-STILT-CLM4.5 and CARVE measurements. **(a)** Observed and simulated monthly CH_4 mole fraction enhancements in 2012 and 2013; **(b)** linear regression of measured versus modeled CH_4 mole fraction enhancements. The error bars are standard deviation of monthly mean.

and those reported in Riley et al. (2011) at the site-level comparison because (1) simulations in this study were done at a higher resolution ($0.5° \times 0.5°$) than those in Riley et al. (2011; $1.9° \times 2.5°$); (2) the current simulations are forced by CRUNCEP climate, while Riley et al. (2011) simulations were forced with Qian et al. (2006) climate; (3) the S parameter is changed, as discussed above; and (4) the overall water and carbon cycles of CLM changed substantially between CLM4.0 and CLM4.5 (Koven et al., 2013). The site-level discrepancies occur because of the uncertainties discussed above and those arising from other parameters (Riley et al., 2011), including Q_{10} of CH_4 production and oxidation, the CH_4 half-saturation oxidation coefficient, the O_2 half-saturation oxidation coefficient, maximum oxidation rate of CH_4 oxidation and the impact of pH and redox potential on CH_4 production.

3.2.2 Regional CH_4 emissions comparison

The biases between CLM4.5 and CarbonTracker CH_4 emissions vary with latitude (Fig. 3). The aggregated F_{S+G} led to larger CH_4 emission biases in Alaska ($\mathrm{RMSE} = 4\,\mathrm{mg\,CH_4\,m^{-2}\,day^{-1}}$) compared to the CH_4 prediction with F_{def} ($\mathrm{RMSE} = 3\,\mathrm{mg\,CH_4\,m^{-2}\,day^{-1}}$), although it led to smaller global CH_4 emission biases. In Alaska between 58 and 66° N during the growing season, CLM4.5 using F_{def} has good agreement with CarbonTracker predictions. In this region, CH_4 emissions begin in May, peak in July and August, and end in October (Fig. 4). In May and June, CarbonTracker shows a weak CH_4 sink ($\sim \mathrm{O}[10^{-2}$–$10^{-1}]\,\mathrm{mg\,CH_4\,m^{-2}\,day^{1}}$) in contrast to a CLM4.5-predicted weak CH_4 source ($\sim \mathrm{O}[10^{-1}]\,\mathrm{mg\,CH_4\,m^{-2}\,day^{-1}}$) with F_{def} and stronger CH_4 source ($\sim \mathrm{O}[1]\,\mathrm{mg\,CH_4\,m^{-2}\,day^{-1}}$) with F_{S+G} in the interior region of Alaska (Interior Alaska) between 63 and 66° N . We hypothesize that this discrep-

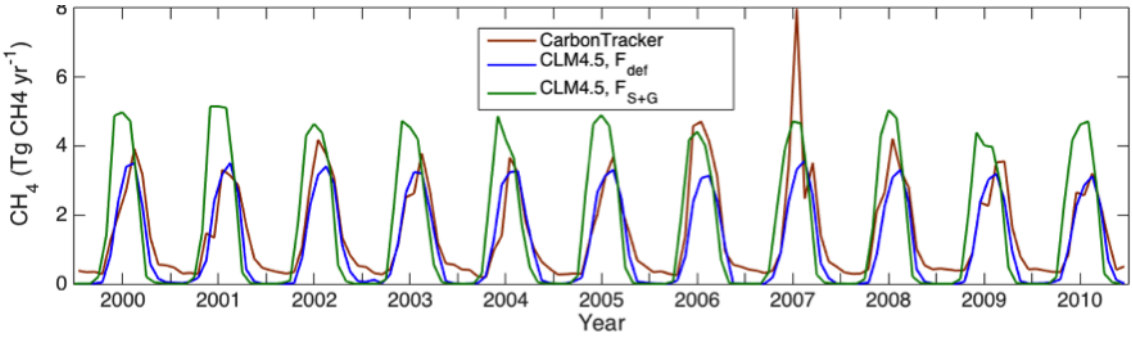

Figure 6. Time variation of integrated CH_4 ($Tg\,CH_4\,yr^{-1}$) emissions from Alaska by CarbonTracker (brown), CLM4.5 with internally predicted fraction of inundation F_{def} (blue) and CLM4.5 SWAMPS-GLWD fraction of inundation F_{S+G} (green).

ancy occurs because of the difference in the two wetland datasets and the accounting of CH_4 emissions from the non-inundated areas in CarbonTracker. Net CH_4 consumption occurs at dry sites where oxygen is available in the topsoil layers (Wickland et al., 1999); however, CH_4 fluxes from the non-inundated, areas which could be substantial (Zona et al., 2016), are excluded in CLM4.5 predictions shown in Fig. 3, as described in the "Methods" section. Interior Alaska has a highly continental climate with warm and relatively dry summers and extremely cold winters. The weak CH_4 source in the dry summer is thus caused by a reduced wetland extent in Interior Alaska. Interior Alaska experiences the most rain events in autumn, mainly in August and September (Hinzman et al., 2006), which restores some of the extent of wetlands and leads to increases in CH_4 emissions in August and early September. CarbonTracker successfully represented the restored wetland in August and September but not CLM4.5 (Figs. 3 and 4). The autumn emission period is very short and ends with the onset of winter, resulting in a strong drop in CH_4 emissions in October.

The CLM4.5 underestimation of northern (> 68° N) Alaska site-level CH_4 emissions during the growing season at some sites is confirmed with comparison to CarbonTracker inversions (Fig. 3b). In southern and northern coastal Alaska, CLM4.5 predicts a much shorter CH_4 emission season and a smaller magnitude of CH_4 emissions than CarbonTracker. The period of the largest underestimation by CLM4.5 is from May to July, with the maximum underestimation of about $9.2\,mg\,CH_4\,m^{-2}\,day^{-1}$ in June. The underestimated CH_4 emissions occur with both F_{S+G} and F_{def} in the north of 68° N. During the cold season from October to April, CLM4.5 predictions with F_{S+G} or F_{def} are consistently smaller than CarbonTracker estimates across all the latitudes. The mean underestimation of cold-season CH_4 emission is less than $1\,mg\,CH_4\,m^{-2}\,day^{-1}$, which is much smaller than the underestimation we found compared to site-level measurements. In comparison with CarbonTracker, CLM4.5 predicted 0.46 ± 0.07 and 0.39 ± 0.08 Tg less Alaska-wide CH_4 emissions in the cold season (October to April) with F_{S+G} and F_{def}, respectively.

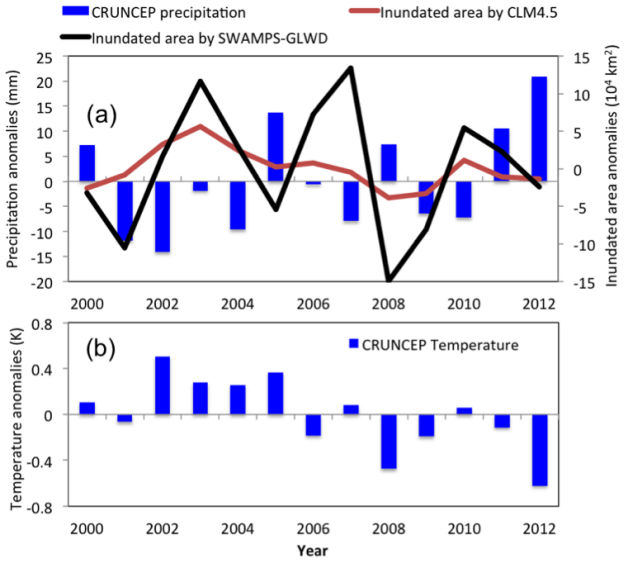

Figure 7. The anomalies of annual precipitation and inundated area in Alaska **(a)** and the anomalies of annual mean temperature **(b)**. The anomalies are calculated by subtracting the average between 2000 and 2012.

The CarbonTracker inversions suggest that 21.9 ± 3.2 % of the annual Alaska CH_4 emissions occur during the cold season, while CLM4.5 predicts that only 3.5 ± 1.3 and 8.3 ± 3.0 % (with F_{def} and F_{S+G}, respectively) occur during the cold season. When September and April are included in the "cold season", the contribution is increased to 45.3 ± 4.5 % by CarbonTracker, which is slightly smaller than the cold-season contribution (50 ± 9 %) inferred from site-level (BEO2, BES, CMDL, ATQ and IVO) measurements (Zona et al., 2016). The September–April contributions to annual emissions predicted by CLM4.5 are 32.1 ± 8.1 and 40.1 ± 14.7 % of the predicted annual emissions with F_{S+G} and F_{def}, respectively. Although CH_4 fluxes from the ocean surface are excluded, we cannot exclude some influence of coastal grid cells on the CarbonTracker estimates.

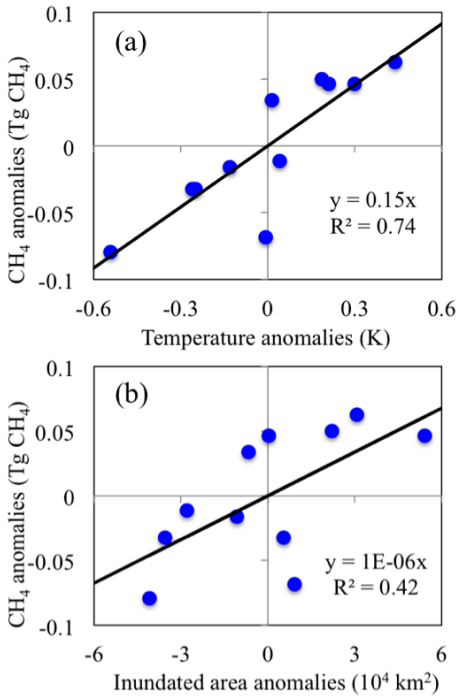

Figure 8. The correlation between CLM-predicted annual CH_4 emission anomalies and mean annual temperature anomalies **(a)** and correlation between annual CH_4 emission anomalies and predicted inundated area anomalies during 2000–2010. The anomalies are calculated by subtracting the average between 2000 and 2010.

The atmospheric CH_4 mole fraction enhancements calculated from CLM4.5-predicted CH_4 emissions are lower than the CARVE-measured CH_4 mole fraction enhancements (Fig. 5). However, in contrast to the emission underestimations that only occur from May to July, the monthly atmospheric CH_4 mole fraction enhancements are underestimated throughout the year, with a maximum underestimation in August (Fig. 5a). The CARVE-measured peak mole fraction enhancement due to surface CH_4 emissions is in August for both 2012 and 2013. Although CLM4.5 predicted the peak CH_4 mole fraction enhancement in August 2012, predicted seasonal CH_4 mole fraction enhancements are much smaller in 2013 and peaks in September. The underestimation of cold-season mole fraction CH_4 enhancements by CLM4.5 leads to 24.0 ± 9.2 and 18.9 ± 17.3 ppb lower CH_4 mole fraction enhancements in April and October 2013, respectively. From April to October, the 2-year mean monthly atmospheric CH_4 mole fraction enhancements are underestimated by 15 ppb in WRF-STILT-CLM model predictions. The underestimation may not be attributed to anthropogenic CH_4 source and agricultural waste because (1) we excluded both observed and modeled CH_4 mole fraction enhancements when $[CO] > 150$ ppb, given that anthropogenic CH_4 mole fraction enhancements are consistently correlated to CO mole fraction enhancements (Zona et al., 2016), and (2) the CH_4 emissions from agricultural waste does not show strong seasonal variation according to CarbonTracker estimates. The large standard deviation of CARVE-observed CH_4 mole fraction enhancements implies that the CH_4 emissions have large spatial and temporal variability. The CLM4.5 predictions are generally within the observed range of variation except in April and May in 2013.

The very low cold-season CH_4 emission predictions on site and regional scales occur because of the assumed temperature sensitivity for CH_4 production when the soil temperature of a given layer is at or below freezing (i.e., no CH_4 production occurs in that soil layer). The multilayer structure of CLM4.5 can in principle generate CH_4 emissions deeper in the soil after the surface has frozen, though even then, modeled diffusion rates through frozen surface layers are low. Although the measurements show winter CH_4 emissions, it remains uncertain whether these emissions are from production at low temperature or residual CH_4 from the end of the growing season. Understanding which of these is occurring is important for diagnosing how to improve model representation of the processes responsible for the wintertime fluxes. The cold-season underestimation by CLM4.5 is also partly attributed to the low wetland area during this period at high latitudes (currently, F_{def} is set to zero when snow is present). Given the current observations of CH_4 emissions during the cold season, we believe these two factors need to be reevaluated in CLM4.5.

3.3 Interannual variation of CH_4 cycle

The CLM4.5 simulated Alaska CH_4 emissions using F_{def} are in very good agreement with CarbonTracker-CH_4 emission in the growing season but biased in the cold season (Fig. 6). The largest growing season discrepancies occur in 2006 and 2007. Bruhwiler et al. (2014) attributed the CarbonTracker 2007 CH_4 emission anomaly to warmer temperatures and higher than normal precipitation. However, the CRUNCEP reanalysis data we used to force CLM4.5 do not have a positive precipitation anomaly in either 2006 or 2007 (Fig. 7a). In contrast, there is a strong negative precipitation anomaly in 2007. The obvious wet years (2000, 2005, 2008, 2011 and 2012) in the CRUNCEP reanalysis data are not directly related to the predicted and measured wetland area anomaly or CH_4 emission anomaly. The mean air temperature in 2007 is only slightly higher than 2000–2012 mean air temperature (Fig. 7b). The correlation analysis implies that the model-predicted interannual CH_4 variation is mainly explained by temperature variation (Fig. 8a; $r = 0.86$, $P = 0.0007$), followed by the default wetland extent (F_{def}) variation (Fig. 8b; $r = 0.65$, $P = 0.03$), but weakly explained by SWAMPS-GLWD wetland extent (F_{S+G}) variation ($r = 0.44$, $P = 0.17$) and precipitation variation ($r = 0.18$, $P = 0.58$). When the CH_4 predictions are calculated with F_{S+G}, correlation between the interannual variation of CH_4 and variation in F_{S+G} ($r = 0.18$,

$P = 0.59$), precipitation ($r = 0.36$, $P = 0.29$) and temperature ($r = 0.32$, $P = 0.33$) are substantially reduced. Interannual variation of CH_4 emissions by CarbonTracker are not well correlated to SWAMPS-GLWD wetland extent variation (r=0.33, P=0.32), variations in CRUNCEP temperature ($r = -0.23$, $P = 0.49$) or precipitation ($r = -0.06$, $P = 0.86$).

4 Concluding remarks

We implemented and tested needed changes to the estimate of aerenchyma area in CLM4.5. The modeled and measured CH_4 emissions and enhancements in atmospheric mole fractions of CH_4 are used to analyze the seasonal wetland CH_4 emission cycle in Alaska. Both the measurements and model predictions show large latitudinal variability of CH_4 seasonal cycles. At the site level, CLM4.5 generally captures the seasonality in growing season CH_4 emissions. However, comparing eddy covariance CH_4 observations with the model predictions is complicated by the unknown fraction of inundation in the footprint of the measurement tower, which may cause large variations in CH_4 emission predictions. Measurements from the sites experiencing wintertime soil frost imply that CH_4 emissions continue in the cold season (October to April). The likely incorrect treatment of CH_4 production under soil frost in CLM4.5 leads to underestimates of the wintertime emissions. This conclusion is confirmed by the discrepancies between CLM4.5 and CarbonTracker predictions, although the cold-season discrepancies between CLM4.5 and CarbonTracker are much smaller than the discrepancies between CLM4.5 and site-level measurements. The differences between the seasonality predicted by CLM4.5 and CarbonTracker vary with time and latitude, although the Alaska area-integrated CH_4 emissions agree well. Besides the strength of wintertime CH_4 emissions, the main discrepancies between CLM4.5 and CarbonTracker estimates are northern and southern coastal area CH_4 emissions. The inundation area leads to uncertainties in predictions of seasonal and interannual variability of CH_4 emissions. Compared with the CLM4.5-predicted inundation area, the aggregated F_{S+G} inundation led to smaller global CH_4 emission biases than F_{def} (RMSE dropped from 3.1 to 2.5 mg CH_4 m^{-2} day^{-1}) between CLM4.5 and CarbonTracker. In contrast, the F_{S+G} inundation area increased seasonal emission biases in Alaska by increasing RMSE from 3 to 4 mg CH_4 m^{-2} day^{-1} compared with the CLM4.5-predicted inundation. The larger SWAMPS-GLWD inundation area leads to much stronger Alaska-wide annual CH_4 emissions compared to those calculated from the default predicted inundation area. CLM4.5 predictions show that the interannual variations of CH_4 emissions are correlated with the reanalysis air temperature and wetland extent variation. In contrast, interannual variation in CarbonTracker CH_4 emissions is weakly related to interannual variation in SWAMPS-GLWD wetland area and reanalysis precipitation and temperature.

The CLM4.5 CH_4 module constrained from global total annual CH_4 emissions does not accurately represent the seasonal cycles in the regional- and site-scale seasonal cycles due to large temporal and spatial heterogeneity in surface CH_4 emissions and wetland extent. Further improving the CH_4 biogeochemical model on the seasonal and annual timescales requires further extensive experiments to better understand climate controls on above- and belowground physiological processes and how vegetation controls gaseous transport (e.g., CH_4 production under low temperatures). Although cold-season site-level measurements are rare, the large discrepancies in winter emissions between CLM4.5 and CarbonTracker predictions and site measurements indicate that studies on winter ecosystem activities and wetland evolution at high latitude would be valuable.

5 Data availability

The CLM4.5 model is released in CESM1.2.2 package available at http://www.cesm.ucar.edu/models/cesm1.2/tags/index.html#CESM1_2_2. The model outputs of CH_4 emission and the fraction of inundation during 2000–2012 are available upon request to the corresponding author.

The site measurement data are available from the publications or the principle investigators provided in the Supplement.

The NOAA CarbonTracker-CH4 data assimilation product is available at http://www.esrl.noaa.gov/gmd/ccgg/carbontracker-ch4/.

The CARVE flight data of CH_4 measurements in 2012 and 2013 are available at https://ilma.jpl.nasa.gov/portal/.

The forcing CRU-NCEP v5 data are available at http://esgf.extra.cea.fr/thredds/fileServer/store/p529viov/cruncep/readme.htm.

The Supplement related to this article is available online at doi:10.5194/bg-13-5043-2016-supplement.

Acknowledgements. Funding for this study was provided by the US Department of Energy, BER, under the RGCM program and NGEE-Arctic project under contract no. DE-AC02-05CH11231. We thank the CARVE flight group for their efforts on CARVE science flights. CarbonTracker CH_4 results provided by NOAA ESRL, Boulder, Colorado, USA, from the website at http://www.esrl.noaa.gov. The eddy covariance tower data used in this study were supported by the Division of Polar Programs of the National Science Foundation (NSF; Award 1204263); Carbon in Arctic Reservoirs Vulnerability Experiment (CARVE), an Earth Ventures (EV-1) investigation, under contract with the National Aeronautics and Space Administration; and Department of Energy (DOE) Grant

DE-SC005160. Logistical support was funded by the NSF Division of Polar Programs.

Edited by: A. V. Eliseev
Reviewed by: two anonymous referees

References

Bartlett, K. B., Crill, P. M., Sass, R. L., Harriss, R. C., and Dise, N. B.: Methane emissions from tundra environments in the Yukon-Kuskokwim delta, Alaska, J. Geophys. Res., 97, 16645–16660, 1992.

Bergamaschi, P., Frankenberg, C., Meirink, J. F., Krol, M., Villani, M. G., Houweling, S., Dentener, F., Dlugokencky, E. J., Miller, J. B., Gatti, L. V., Engel, A., and Levin, I.: Inverse modeling of global and regional CH_4 emissions using SCIAMACHY satellite retrievals, J. Geophys. Res.-Atmos., 114, D22301, doi:10.1029/2009JD012287, 2009.

Billings, W. D., Peterson, K. M., Shaver, G. R., and Trent, A. W.: Root growth, respiration, and carbon dioxide evolution in an Arctic tundra soil, Arct. Alp. Res., 9, 129–137, 1977.

Bohn, T. J., Melton, J. R., Ito, A., Kleinen, T., Spahni, R., Stocker, B. D., Zhang, B., Zhu, X., Schroeder, R., Glagolev, M. V., Maksyutov, S., Brovkin, V., Chen, G., Denisov, S. N., Eliseev, A. V., Gallego-Sala, A., McDonald, K. C., Rawlins, M. A., Riley, W. J., Subin, Z. M., Tian, H., Zhuang, Q., and Kaplan, J. O.: WETCHIMP-WSL: intercomparison of wetland methane emissions models over West Siberia, Biogeosciences, 12, 3321–3349, doi:10.5194/bg-12-3321-2015, 2015.

Brouchkov, A., Fukuda, M., Tomita, F., Asano, K., and Tanaka, M.: Microbiology and gas emission at low temperatures: some field and experimental results, Töhoku Geophys. Journ., 36, 452–455, 2003.

Bruhwiler, L., Dlugokencky, E., Masarie, K., Ishizawa, M., Andrews, A., Miller, J., Sweeney, C., Tans, P., and Worthy, D.: CarbonTracker-CH_4: an assimilation system for estimating emissions of atmospheric methane, Atmos. Chem. Phys., 14, 8269–8293, doi:10.5194/acp-14-8269-2014, 2014.

Chan, K. M. and Wood, R.: The seasonal cycle of planetary boundary layer depth determined using COSMIC radio occultation data, J. Geophys. Res.-Atmos., 118, 12422–12434, doi:10.1002/2013JD020147, 2013.

Chang, R. Y. W, Miller, C. E., Dinardo, S. J., Karion, A., Sweeney, C., Daube, B., Henderson, J. M., Mountain, M. E., Eluszkiewicz, J., Miller, J. B., Bruhwiler, L. M. P., and Wofsy, S. C.: Methane emissions from Alaska in 2012 from CARVE airborne observations, P. Natl. Acad. Sci. USA, 111, 16694–16699, 2014.

Chapin, F. S.: Morphological and physiological mechanisms of temperature compensation in phosphate absorption along a latitudinal gradient, Ecology, 55, 1180–1198, 1974.

Clein, J. S. and Schimel, J. P.: Microbial activity of tundra and taiga soils at sub-zero temperatures, Soil. Biol. Biochem., 29, 1231–1234, 1995.

Comas, X., Slater, L., and Reeve, A.: Seasonal geophysical monitoring of biogenic gases in a northern peatland: implications for temporal and spatial variability in free phase gas production rates, J. Geophys. Res.-Biogeo., 113, G01012, doi:10.1029/2007JG000575, 2008.

Dunfield, P., Knowles, R., Dumont, R., and Moore, T. R.: Methane production and consumption in temperate and subarctic peat soils: Response to temperature and pH, Soil Biol. Biochem., 25, 321–326, 1993.

Euskirchen, E. S., Bret-Harte, M. S., Scott, G. J., Edgar, C., and Shaver, G. R.: Seasonal patterns of carbon dioxide and water fluxes in three representative tundra ecosystems in northern Alaska, Ecosphere, 3, 1–19, 2012.

Hargreaves, K. J., Fowler, D., Pitcairn, C. E. R., and Aurela, M.: Annual methane emission from Finnish mires estimated from eddy covariance campaign measurements, Theor. Appl. Climatol. 70, 203–213, 2001.

Henderson, J. M., Eluszkiewicz, J., Mountain, M. E., Nehrkorn, T., Chang, R. Y.-W., Karion, A., Miller, J. B., Sweeney, C., Steiner, N., Wofsy, S. C., and Miller, C. E.: Atmospheric transport simulations in support of the Carbon in Arctic Reservoirs Vulnerability Experiment (CARVE), Atmos. Chem. Phys., 15, 4093–4116, doi:10.5194/acp-15-4093-2015, 2015.

Hinzman, L. D., Viereck, L. A., Adams, P., Romanovsky, V. E., and Yoshikawa, K.: Climate and permafrost dynamics of the Alaskan boreal forest, in: Alaska's changing boreal forest, edited by: Chapin III, F. S., Oswood, M. W., Van Cleve, K., Viereck, L. A., and Verbyla, D. L., Oxford University Press, New York, 39–61, 2006.

Hommeltenberg, J., Schmid, H. P., Drösler, M., and Werle, P.: Can a bog drained for forestry be a stronger carbon sink than a natural bog forest?, Biogeosciences, 11, 3477–3493, doi:10.5194/bg-11-3477-2014, 2014.

Hugelius, G., Strauss, J., Zubrzycki, S., Harden, J. W., Schuur, E. A. G., Ping, C.-L., Schirrmeister, L., Grosse, G., Michaelson, G. J., Koven, C. D., O'Donnell, J. A., Elberling, B., Mishra, U., Camill, P., Yu, Z., P almtag, J., and Kuhry, P.: Estimated stocks of circumpolar permafrost carbon with quantified uncertainty ranges and identified data gaps, Biogeosciences, 11, 6573–6593, doi:10.5194/bg-11-6573-2014, 2014.

Iversen, C. M., Sloan, V. L., Sullivan, P. F., Euskirchen, E. S., McGuire, A. D., Norby, R. J., Walker, A. P., Warren, J. M., and Wullschleger, S. D.: The unseen iceberg: plant roots in arctic tundra, New Phytol., 205, 34–59, doi:10.1111/nph.13003, 2015.

Iwata, H., Harazono, Y., Ueyama, M., Sakabe, A., Nagano, H., Kosugi, Y., Takahashi, K., and Kim, Y.: Methane exchange in a poorly-drained black spruce forest over permafrost observed using the eddy covariance technique, Agr. Forest Meteorol., 214–215, 157–168, 2015.

Juutinen, S., Alm, J., Larmola, T., Huttunen, J. T., Morero, M., Martikainen, P. J., and Silvola, J.: Major implication of the littoral zone for methane release from boreal lakes, Global Biogeochem. Cy., 17, 1117, 10.1029/2003GB002105, 2003.

King, J. Y., William, S. R., and Shannon K. R.: Methane emission and transport by arctic sedges in Alaska: results of a vegetation removal experiment, J. Geophys. Res., 103, 29083–29092, 1998.

Kirschke, S., Bousquet, P., Ciais, P., Saunois, M., Canadell, J. G., Dlugokencky, E. J., Bergamaschi, P., Bergmann, D., Blake, D. R., Bruhwiler, L., Cameron Smith, P., Castaldi, S., Chevallier, F., Feng, L., Fraser, A., Heimann, M., Hodson, E. L., Houweling, S., Josse, B., Fraser, P. J., Krummel, P. B., Lamarque, J., Langenfelds, R. L., Le Quéré, C., Naik, V., O'Doherty, S., Palmer, P. I., Pison, I., Plummer, D., Poulter, B., Prinn, R. G., Rigby, M., Ringeval, B., Santini, M., Schmidt, M., Shindell, D. T., Simp-

son, I. J., Spahni, R., Steele, L. P., Strode, S. A., Sudo, K., Szopa, S., van der Werf, G. R., Voulgarakis, A., van Weele, M., Weiss, R. F., Williams, J. E., and Zeng, G.: Three decades of global methane sources and sinks, Nat. Geosci., 6, 813–823, doi:10.1038/ngeo1955, 2013.

Koven, C. D., Riley, W. J., Subin, Z. M., Tang, J. Y., Torn, M. S., Collins, W. D., Bonan, G. B., Lawrence, D. M., and Swenson, S. C.: The effect of vertically resolved soil biogeochemistry and alternate soil C and N models on C dynamics of CLM4, Biogeosciences, 10, 7109–7131, doi:10.5194/bg-10-7109-2013, 2013.

Kummerow, J. and Russell, M.: Seasonal root growth in the Arctic tussock tundra, Oecologia, 47, 196–199, 1980.

Lehner, B. and Doll, P.: Development and validation of a global database of lakes, reservoirs and wetlands, J. Hydrol., 296, 1–22, 2004.

Lupascu, M., Wadham, J. L., Hornibrook, E. R. C., and Pancost, R. D.: Temperature sensitivity of methane production in the permafrost active layer at Stordalen, Sweden: A comparison with non-permafrost northern wetlands, Arct. Antarc. Alp. Res., 44, 469–482, 2012.

Mastepanov, M., Sigsgaard, C., Tagesson, T., Ström, L., Tamstorf, M. P., Lund, M., and Christensen, T. R.: Revisiting factors controlling methane emissions from high-Arctic tundra, Biogeosciences, 10, 5139–5158, doi:10.5194/bg-10-5139-2013, 2013.

Mastepanov, M., Sigsgaard, C., Dlugokencky, E. J., Houweling, S., Ström L., Tamstorf, M. P., and Christensen, T. R.: Large tundra methane burst during onset of freezing, Nature, 456, 628–631, 2008.

McEwing, K. R., Fisher, J. P., and Zona, D.: Environmental and vegetation controls on the spatial variability of CH_4 emission from wet-sedge and tussock tundra ecosystem in the Arctic, Plant Soil, 388, 37–52, 2015.

Melton, J. R., Wania, R., Hodson, E. L., Poulter, B., Ringeval, B., Spahni, R., Bohn, T., Avis, C. A., Beerling, D. J., Chen, G., Eliseev, A. V., Denisov, S. N., Hopcroft, P. O., Lettenmaier, D. P., Riley, W. J., Singarayer, J. S., Subin, Z. M., Tian, H., Zürcher, S., Brovkin, V., van Bodegom, P. M., Kleinen, T., Yu, Z. C., and Kaplan, J. O.: Present state of global wetland extent and wetland methane modelling: conclusions from a model intercomparison project (WETCHIMP), Biogeosciences, 10, 753–788, doi:10.5194/bg-10-753-2013, 2013.

Meng, L., Hess, P. G. M., Mahowald, N. M., Yavitt, J. B., Riley, W. J., Subin, Z. M., Lawrence, D. M., Swenson, S. C., Jauhiainen, J., and Fuka, D. R.: Sensitivity of wetland methane emissions to model assumptions: application and model testing against site observations, Biogeosciences, 9, 2793–2819, doi:10.5194/bg-9-2793-2012, 2012.

Mialon, A., Royer, A., and Fily, M.: Wetland seasonal dynamics and interannual variability over northern high latitudes, derived from microwave satellite data, J. Geophys. Res., 110, D17102, doi:10.1029/2004JD005697, 2005.

Moosavi, S. C., Crill, P. M., Pullman, E. R., Funk, D. W., and Peterson, K. M.: Controls on CH_4 flux from an Alaskan boreal wetland, Global Biogeochem. Cy., 10, 287–296, 1996.

Morin, T. H., Bohrer, G., Naor-Azrieli, L., Mesi, S., Kenny, W. T., Mitsch, W. J., and Schäfer, K. V. R.: The seasonal and diurnal dynamics of methane flux at a created urban wetland, Ecol. Engin., 72, 74–83, 2014.

Peters, W., Jacobson, A. R., Sweeney, C., Andrews, A. E., Conway, T. J., Masarie, K., Miller, J. B., Bruhwiler, L. M. P., Petron, G., Hirsch, A., Worthy, D. E. J., van der Werf G. R., Randerson, J. T., Wennberg, P. O., Krol, M. C., and Tans, P. P.: An Atmospheric perspective on north American carbon dioxide exchange: CarbonTracker, P. Natl. Acad. Sci. USA, 18925–18930, 2007.

Pickett-Heaps, C. A., Jacob, D. J., Wecht, K. J., Kort, E. A., Wofsy, S. C., Diskin, G. S., Worthy, D. E. J., Kaplan, J. O., Bey, I., and Drevet, J.: Magnitude and seasonality of wetland methane emissions from the Hudson Bay Lowlands (Canada), Atmos. Chem. Phys., 11, 3773–3779, doi:10.5194/acp-11-3773-2011, 2011.

Prigent, C., Papa, F., Aires, F., Rossow, W. B., and Matthews, E.: Global inundation dynamics inferred from multiple satellite observations, 1993–2000, J. Geophys. Res.-Atmos., 112, D12107, doi:10.1029/2006JD007847, 2007.

Qian, T. T., Dai, A., Trenberth, K. E., and Oleson, K. W.: Simulation of global land surface conditions from 1948 to 2004, Part I: Forcing data and evaluations, J. Hydrometeorol., 7, 953–975, 2006.

Riley, W. J., Subin, Z. M., Lawrence, D. M., Swenson, S. C., Torn, M. S., Meng, L., Mahowald, N. M., and Hess, P.: Barriers to predicting changes in global terrestrial methane fluxes: analyses using CLM4Me, a methane biogeochemistry model integrated in CESM, Biogeosciences, 8, 1925–1953, doi:10.5194/bg-8-1925-2011, 2011.

Ringeval, B., de Noblet-Ducoudré, N., Ciais, P., Bousquet, P., Prigent, C., Papa, F., and Rossow, W. B.: An attempt to quantify the impact of changes in wetland extent on methane emissions on the seasonal and interannual time scales, Global Biogeochem. Cy., 24, GB2003, doi:10.1029/2008GB003354, 2010.

Rinne, J., Riutta, T., Pihlatie, M., Aurela, M., Haapanala, S., Tuovinen, J., and Tuittila, E.: Annual cycle of methane emission from a boreal fen measured by the eddy Covance technique, Tellus, 59B, 449–457, 2007.

Roulet, N. T., Ash, R., and Moore, T. R.: Low boreal wetlands as a source of atmospheric methane, J. Geophys. Res., 97, 3739–3749, 1992.

Schroeder, R., McDonald K. C., Champan, B. D., Jensen, K., Podest, E., Tessler, Z. D., Bohn, T. J., and Zimmermann, R.: Development and evaluation of a multi-year fractional surface water data set derived from active/passive microwave remote sensing data, 7, 16688–16732, 2015.

Segers, R.: Methane production and methane consumption: a review of process underlying wetland methane fluxes, Biogeochemistry, 41, 23–51,1998.

Sloan, V.: Plant roots in Arctic ecosystems: stocks and dynamics and their coupling to aboverground parameters, PhD Thesis, University of Sheffield, Sheffield, UK, 2011.

Song, C., Xu, X., Sun, X., Tian, H., Sun, L., Miao, Y., Wang, X., and Guo, Y.: Large methane emission upon spring thaw from natural wetlands in the northern permafrost region, Environ. Res. Lett., 7, 034009, doi:10.1088/1748-9326/7/3/034009, 2012.

Sturtevant, C. S., Oechel, W. C., Zona, D., Kim, Y., and Emerson, C. E.: Soil moisture control over autumn season methane flux, Arctic Coastal Plain of Alaska, Biogeosciences, 9, 1423–1440, doi:10.5194/bg-9-1423-2012, 2012.

Sullivan, P. F. and Welker, J. M.: Warming chambers stimulate early season growth of an arctic sedge: results of a minirhizotron field study, Oecologia, 142, 616–626, 2005.

Tian, Y, Dickinson, R. E., Zhou, L., Zeng, X., Dai, Y., Myneni, R. B., Knyazikhin, Y., Zhang, X., Friedl, M., Yu, H., Wu, W., and Shaikh, M.: Comparison of seasonal and spatial variations of leaf area index and fraction of absorbed photosynthetically active radiation from Moderate Resolution Imaging Spectroradiometer (MODIS) and Common Land Model, J. Geophys. Res., 109, D01103, doi:10.1029/2003JD003777, 2004.

Tokida, T., Mizoguchi, M., Miyazaki, T., Kagemoto, A., Nagata, O., and Hatano, R.: Episodic release of methane bubbles from peatland during spring thaw, Chemosphere, 70, 165–171, 2007.

Torn, M. S. and Chapin III, F. S.: Environmental and biotic controls over methane flux from arctic tundra, Atmos. Environ., 32, 3201–3218, 1993.

van Fischer, J. C., Rhew, R. C., Ames, G. M., Fosdick, B. K., and von Fischer, P. E.: Vegetation height and other controls of spatial variability in methane emissions from the Arctic coastal tundra at Barrow, Alaska, J. Geophys. Res., 115, G00I03, doi:10.1029/2009JG001283, 2010

van Hulzen J. B., Segers, R., van Bodegom, P. M., and Leffelaar, P. A.: Temperature effects on soil methane production: and explanation for observed variability, Soil Biol. Biochem., 31, 1919–1929, 1999.

van Winden, J. F., Reichart, G.-J., McNamara, N. P., Benthien, A., and Damsté, J. S. S.: Temperature-induced increase in methane release from peat bogs: a mesocosm experiment, PLoS ONE 7, e39614, doi:10.1371/journal.pone.0039614, 2012.

Wania, R., Ross, I., and Prentice, I. C.: Implementation and evaluation of a new methane model within a dynamic global vegetation model: LPJ-WHyMe v1.3.1, Geosci. Model Dev., 3, 565–584, doi:10.5194/gmd-3-565-2010, 2010.

Whalen, S. C. and Reeburgh, W. S.: Consumption of atmospheric methane by tundra soils, Nature, 342, 160–162, 1990.

Wickland, K. P., Striegl, R. G., Schmidt, S. K., and Mast, M. A.: Methane flux in subalpine wetland and unsaturated soils in the southern Rocky Mountains, Global Biogeochem. Cy., 13, 101–113, 1999.

Wilson, J. O., Crill, P. M., Bartlett, K. B., Sebacher, D. I., Harriss, R. C., and Sass, R. L.: Seasonal variation of methane emissions from a temperate swamp, Biogeochemistry, 8, 55–71, 1998.

Yvon-Durocher, G., Allen, A. P., Bastviken, D., Conrad, R., Gudasz, C., St-Pierre, A., Thanh-Duc, N., and del Giorgio, P. A.: Methane fluxes show consistent temperature dependence across microbial to ecosystem scale, Nature, 507, 488–491, 2014.

Zhuang, Q., Melillo, J. M., Kicklighter, D. W., Prinn, R. G., McGuire, A. D., Steudler, P. A., Felzer, B. S., and Hu, S.: Methane fluxes between terrestrial ecosystems and the atmosphere at northern high latitudes during the past century: A retrospective analysis with a process based biogeochemistry model, Global Biogeochem. Cy., 18, GB3010, doi:3010.1029/2004GB002239, 2004.

Zona, D., Gioli, B., Commane, R., Lindaas, J., Wofsy, S. C., Miller, C. E., Dinardo, S. J., Dengel, S., Sweeney, C., Karion, A., Chang, R.Y.-W., Henderson, J. M., Murphy, P. C., Goodrich, J. P., Moreaux, V., Liljedahl, A., Watts, J. D., Kimball, J. S., Lipson, D. A., and Oechel, W. C.: Cold season emissions dominate the Arctic tundra methane budget, P. Natl. Acad. Sci. USA, 113, 40–45, 2016.